Oceanic response to the consecutive Hurricanes Dorian and Humberto (2019) in the Sargasso Sea

Dailé Avila-Alonso[1,2], Jan M. Baetens[2], Rolando Cardenas[1], and Bernard De Baets[2]

[1]Laboratory of Planetary Science, Department of Physics, Universidad Central "Marta Abreu" de Las Villas, 54830, Santa Clara, Villa Clara, Cuba
[2] KERMIT, Department of Data Analysis and Mathematical Modelling, Faculty of Bioscience Engineering, Ghent University, 9000 Ghent, Belgium

Correspondence: Dailé Avila-Alonso (davila@uclv.cu)

Abstract. Understanding the oceanic response to tropical cyclones (TCs) is of importance for studies on climate change. Although the oceanic effects induced by individual TCs have been extensively investigated, studies on the oceanic response to the passage of consecutive TCs are rare. In this work, we assess the upper oceanic response to the passage of the Hurricanes Dorian and Humberto over the western Sargasso Sea in 2019 using satellite remote sensing and modelled data. We found that
5 the combined effects of these slow-moving TCs led to an increased oceanic response during the third and fourth post-storm weeks of Dorian (accounting for both Dorian and Humberto effects) because of the induced mixing and upwelling at this time. Overall, anomalies of sea surface temperature, ocean heat content and mean temperature from the sea surface to a depth of 100 m were a 50, 63 and 57% smaller (more negative) in the third/fourth post-storm weeks than in the first/second post-storm weeks (accounting only for Dorian effects) of Dorian, respectively, while surface chlorophyll-a (chl-a) concentration
10 anomalies, the mean ch-a concentration in the euphotic zone and the chl-a concentration in the deep chlorophyll maximum were 16, 4 and 16% higher in the third/fourth post-storm weeks than in the first/second post-storm weeks, respectively. The sea surface cooling and increased biological response induced by these TCs were significantly higher (Mann-Whitney test $p < 0.05$) as compared to climatological records. Our climatological analysis reveals that the strongest TC-induced oceanographic variability in the western Sargasso Sea can be associated with the occurrence of consecutive TCs and long-lasting TC forcing.

15   **Keywords:** Chlorophyll-a concentration, sea surface temperature, tropical cyclones

1   Introduction

Hurricanes and typhoons (or more generally, tropical cyclones (TCs)) are among the most destructive natural phenomena on Earth leading to great social and economic losses (Welker and Faust, 2013; Lenzen et al., 2019), as well as ecological perturbations of both marine and terrestrial ecosystems (Fiedler et al., 2013; de Beurs et al., 2019; Lin et al., 2020). Given the
20 devastating effects of TCs, the question of how they will be affected by climate change has received considerable scientific attention (Henderson-Sellers et al., 1998; Knutson et al., 2010; Walsh et al., 2016). Modelling studies project either a decrease in TC frequency accompanied by an increased frequency of the strongest storms or an increase of the number of TCs in general, depending on the spatial resolution of the models (Knutson et al., 2010; Camargo and Wing, 2016; Walsh et al., 2016; Zhang

et al., 2017; Bacmeister et al., 2018; Bhatia et al., 2018). In any case, an assessment of the impact of climate change on future
25 TC activity needs to be based on whether or not the past and present changes in climate have had a detectable effect on TCs to
date (Walsh et al., 2016).

The ocean is the main source of energy for TC intensification, hence, changes in oceanic environments considerably affect
TC activity (Knutson et al., 2010; Huang et al., 2015; Sun et al., 2017; Trepanier, 2020). Sea surface temperature (SST) and
ocean heat content (OHC) have risen significantly over the past several decades in regions of TC formation (Santer et al., 2006;
30 Defforge and Merlis, 2017; Trenberth et al., 2018; Cheng et al., 2019; Zanna et al., 2019; Chih and Wu, 2020). Accordingly, TC
lifetime maximum intensity significantly increased during 1981–2016 for both the Northern and Southern Hemispheres (Song
et al., 2018). More specifically, both the frequency and intensity of TCs in the North Atlantic basin increased over the past few
decades (Deo et al., 2011; Walsh et al., 2016), while a significant increase in TC intensification rates in the period 1982–2009
has been documented with a positive contribution from anthropogenic forcing (Bhatia et al., 2019).

35 In agreement, the last Atlantic hurricane seasons have shown well-above normal activity (Trenberth et al., 2018; Bang et al.,
2019). For instance, the 2017 hurricane season was extremely active with 17 named storms (1981–2010 median is 12.0),
10 hurricanes (median is 6.5) and 6 major hurricanes (median is 2.0) (Klotzbach et al., 2018). It will be remembered for the
unprecedented devastation caused by the major hurricanes Harvey, Irma and Maria breaking many historical records (Tren-
berth et al., 2018; Bang et al., 2019). This high activity was associated with unusually high SST in the eastern Atlantic region,
40 where many storms developed, together with record-breaking OHC values favouring TC intensification (Lim et al., 2018).
Besides, the 2019 hurricane season was relevant because of the high number of named storms (18 storms) and the develop-
ment of the long-lasting Hurricane Dorian, which broke the record for the strongest Atlantic hurricane outside the tropics
(>23.5°N) (Klotzbach et al., 2019). Two weeks after the passage of Dorian across the western Sargasso Sea, TC Humberto
moved across this area. The interaction of two storms closely related in time and space provides an in situ experiment for
45 studying oceanic response (Baranowski et al., 2014). Although there have been extensive studies investigating the oceanic
response to the passage of individual TCs, the effects induced by consecutive TCs has been much less documented (Wu and
Li, 2018; Ning et al., 2019).

Given that the greatest ocean warming is projected to occur by the end of the century (Cheng et al., 2019), we may anticipate
a further increase in TC intensity and/or frequency. The assessment of the oceanic response to TCs has been a hot topic
50 given its importance for studies on climate change, ecological variability and environmental protection (Fu et al., 2014). More
specifically, insights into the phytoplankton response to severe weather events are essential in order to ascertain the capacity
of the oceans to absorb carbon dioxide through photosynthesis (Davis and Yan, 2004). Hence, several studies have assessed
the oceanic response to recent major hurricanes in the North Atlantic basin (e.g., Trenberth et al., 2018; Miller et al., 2019b;
Avila-Alonso et al., 2020; Hernández et al., 2020) and others in very active hurricane seasons such as in 2005 (e.g., Oey et al.,
55 2006, 2007; Shi and Wang, 2007; Gierach and Subrahmanyam, 2008). In this work, we assess the upper oceanic responses
induced by Hurricanes Dorian and Humberto in the western Sargasso Sea in 2019. This gives insights into the implications of
a simultaneous increase of both the frequency and intensity of TCs in the North Atlantic basin.

2 Materials and Methods

2.1 Study area

60 The Sargasso Sea is the part of the North Atlantic Ocean (known as the North Atlantic gyre) that is bounded by the surrounding clockwise-rotating system of major currents, i.e., the North Atlantic Current on the north, the Gulf Stream on the west, the North Atlantic Equatorial Current on the south, and the Canary Current on the east (Deacon, 1942; Laffoley et al., 2011). Hence, the Sargasso Sea essentially lies between the parallels 20–35°N and the meridians 30–70°W (Augustyn et al., 2013). We specifically focused the western Sargasso Sea, since this area was the area affected by Dorian and Humberto.

2.2 Synoptic history of Dorian and Humberto

65 Dorian originated from a tropical wave that moved off the west coast of Africa on August 19, 2019. The wave crossed the tropical Atlantic becoming a tropical depression on August 24 at 0600 UTC at about 1296 km east-southeast of Barbados and a tropical storm at 1800 UTC that day. Dorian's intensity increased further while moving west-northwest reaching hurricane category by September 27 and major hurricane category by September 30, while being centered about 713 km east of the northwestern Bahamas (Figure 1A). Dorian became a category 5 hurricane on the Saffir-Simpson Hurricane Scale in the north-
70 western Bahamas on September 1 with estimated winds of 296 km h^{-1}. At this time, it moved very slowly westward making landfall on Grand Bahama Island on September 2 with winds of 287 km h^{-1} (Figure 1A). Dorian remained stationary over this area weakening to category 4 and 3 (Figure 1A) because of its interaction with land and the induced-ocean cooling. Then, it turned northwestward and started moving along the east of Florida during the period from 3–5 September as a category 2, but
75 as its core moved over the Gulf Stream, Dorian regained strength and reached category 3 again offshore of the coasts of Georgia and South Carolina (Figure 1A). Afterwards, Dorian made landfall over Cape Hatteras on September 6 with 157 km h^{-1} and left the Sargasso Sea this day, when moving beyond 35°N (Avila et al., 2020).

On the other hand, Humberto primarily originated from a weak tropical wave that started off the west coast of Africa on August 27 and moved westward across the tropical Atlantic approaching the Lesser Antilles on September 4. By September 13 it
80 became a tropical depression east of the central Bahamian island of Eleuthera at 1800 UTC and 6 hours later it became a tropical storm (Figure 1A). Then, Humberto turned northwestward and maintained that direction for the next 48 hours at a slow translation speed. It reached hurricane category on September 16 about 278 km east-northeast of Cape Canaveral, Florida (Figure 1A). At this point, Humberto started to move east-northeastward strengthening to a major hurricane on September 18 (Figure 1A). Thereafter, Humberto weakened steadily and became an extratropical cyclone by September 20 (Stewart, 2020).

2.3 Methodology

85

We analysed the oceanic response along the trajectory of Dorian in 200 km radius semi-disks centered at consecutive hurricane positions in the 20–35°N latitudinal band (limits of the Sargasso Sea) (Figure 1B). We followed this asymmetric approach due to the fact that Dorian moved close to the east coast and shelf waters of the United States of America (USA), so, the waters to
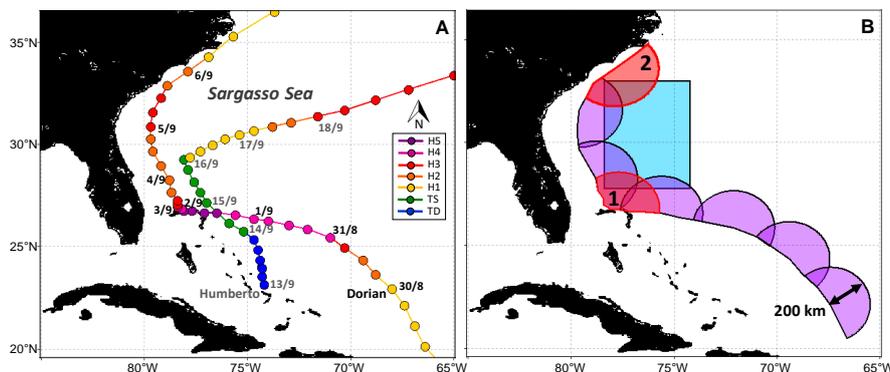
Figure 1. (A) Trajectory of tropical cyclones (TCs) Dorian and Humberto (2019). Colours indicate the TC category (i.e. TD: Tropical depression, TS: Tropical storm, H1–H5: Saffir Simpson Hurricane Categories). Numbers along trajectories indicate the day/month. (B) 200 km semi-disks along Dorian's trajectory and the square area in the western Sargasso Sea. Red semi-disks 1 and 2 indicate the areas where chlorophyll-a concentration profiles were analysed.

the left side of its trajectory can be considered as optically complex waters (i.e., Case 2 waters of the classification of Morel, 90 1980), which limit the use of ocean colour data. On the other hand, coastal/shelf and oceanic waters respond differently to the passage of TCs (Zhao et al., 2015). For instance, coastal areas are strongly affected by freshwater discharge and flooding leading to a high concentration of nutrients and post-storm phytoplankton productivity (Farfán et al., 2014; Paerl et al., 2019). Thus, in order to account for the oceanic response in the Sargasso Sea, we restricted to the deep waters to the right of Dorian's trajectory. Given that upwelling, cooling and deepening of the isothermal layer are more intense on the right side of a TC's trajectory in the Northern Hemisphere (Price, 1981; Hanshaw et al., 2008; Gierach and Subrahmanyam, 2008; Fu et al., 2014), our asymmetric approach captures the strongest oceanic response. Besides these Lagrangian measurements along Dorian's trajectory, we also investigated the oceanic response in a square area (Eulerian) located to the right of its trajectory (Figure 1B), where a considerable post-storm sea surface cooling was observed. The strongest oceanic response accounting for the combined effect of Dorian and Humberto was observed in this square area since it was affected by the intensive winds near the center of Dorian 100 and it was crossed by Humberto. In contrast, the entire area along Dorian's trajectory was affected by Humberto to a lesser extent, especially the waters surrounding Grand Bahama Island since Humberto crossed the semi-disk 1 (see Figure 1). Moreover, storm surge and saltwater inundation were reported along the east coast of Florida following the passage of Humberto (Stewart, 2020), indicating that this area was also exposed to its forces.

We assessed the daily response of the oceanographic variables before, during and after the passage of Dorian. We considered 105 the pre-storm week (i.e., days –10 to –3 before hurricane passage) as a benchmark for comparison with the four post-storm weeks (i.e., from day 0 to 30, where day 0 refers to the day the hurricane entered the study area) in agreement with previous studies (Vincent et al., 2012b; Menkes et al., 2016; Avila-Alonso et al., 2019). For what concerns the square area, we considered day 0 as the day that Dorian started to impact it, i.e., as soon as there was overlap of the 200 km radius semi-disks and the square polygons. Overall, the first two post-storm weeks account for Dorian-induced oceanic effects, while the third and fourth post-

110 storm weeks account for the combined effects of both Dorian and Humberto. Daily arithmetic means of the studied variables
were computed along Dorian's trajectory and in the square study area. For the former, the mean values of the consecutive semi-
disks were averaged to retrieve the daily mean along the entire hurricane trajectory, in agreement with Babin et al. (2004).

2.4 Data

2.4.1 Response variables

115 We considered SST and surface chlorophyll-a (chl-a) concentration as the main physical and biological response variables,
respectively, as in previous studies in the region (e.g., Babin et al., 2004; Shropshire et al., 2016). SST data were derived from
the Operational SST and Sea Ice Analysis (OSTIA) Near Real Time level 4 product (Donlon et al., 2012), provided by the
Copernicus Marine Environment Monitoring Service (CMEMS, *http://marine.copernicus.eu*). OSTIA merges both infrared
and microwave radiometer data, together with in situ observations at a spatial resolution of $0.05° \times 0.05°$.

120 We used the CMEMS GlobColour multisatellite merged data of near real-time chl-a concentration (level 4 cloud free product)
which is based on a spatial and temporal interpolation of the level 3 product at a spatial resolution of $0.0417° \times 0.0417°$ (Gar-
nesson et al., 2019b, a). The chl-a analyses involve multiple chl-a algorithms, i.e., CI algorithm for oligotrophic waters (Hu
et al., 2012) and OC5 algorithm for mesotrophic and coastal waters (Gohin et al., 2002; Gohin, 2011). The CI and OC5 conti-
nuity is ensured using the same approach as that utilized by NASA. When the chl-a concentration is in the range from 0.15 to
125 0.2 mg m^{-3}, a linear interpolation is used (Garnesson et al., 2019b). The algorithm validation has shown a good relationship
between in situ measurements and satellite observations of chl-a concentration, while daily level 4 products in general show a
low bias (0.04) and a coefficient of determination of 0.71 at global scale (Garnesson et al., 2019a).

Moreover, we also investigated the subsurface oceanographic variability by analysing data of the OHC, which corresponds
the integrated thermal energy from the sea surface to 26 °C isotherm depth (Leipper and Volgenau, 1972; Price, 2009), and
130 the average temperature from the sea surface to a depth of 100 m (T_{100}, a typical depth of vertical mixing by a category 3
hurricane) (Price, 2009). The latter has been suggested as an adequate variable to identify subsurface thermal fields (Price,
2009), so we can draw sound conclusions on the subsurface cooling as a consequence of the TCs. Similarly, we analyzed chl-a
concentration profiles to assess the post-storm biological response throughout the euphotic zone (0–200 m).

We used daily OHC data from the Systematically Merged Regional Atlantic Temperature and Salinity (SMARTS) Clima-
135 tology adjusted to a two-layer reduced gravity model at a spatial resolution of $0.25° \times 0.25°$ (Meyers et al., 2014) (data avail-
able at *ftp://ftp.nodc.noaa.gov/pub/data.nodc/sohcs*). SMARTS blends temperature and salinity fields from the World Ocean
Atlas 2001 (WOA01) and the Generalized Digital Environmental Model (GDEM) version 3.0 based on their performance
compared to in situ measurements (Meyers et al., 2014). SMARTS estimations of OHC during hurricane seasons show little
bias and low normalized root mean squared difference (RMSD normalized by the mean of the local in situ observations) in
140 the North Atlantic basin in general, with the lowest values in the western Sargasso Sea (e.g., RMSD≈0.3) (see Figure 2-16 in
Shay et al., 2019). Temperature profiles were derived from the Global Ocean Physics Analysis and Forecasting product at a
spatial resolution of $0.083° \times 0.083°$, provided by Mercator Ocean and distributed by CMEMS. This product uses version 3.1

of the NEMO (Nucleus for European Modelling of the Ocean) ocean model and has 50 vertical levels (22 levels within the upper 100 m) with a decreasing resolution from 1 m at the sea surface to 450 m into the deep ocean (Lellouche et al., 2016).

145   Chl-a profiles were obtained from the CMEMS Global Biogeochemical Analysis and Forecast product of Mercator Ocean. This product is a global biogeochemical simulation result (at $0.25° \times 0.25°$ spatial resolution) obtained using the PISCES (Pelagic Interactions Scheme for Carbon and Ecosystem Studies) model which is part of the NEMO model (Lamouroux et al., 2019). The vertical grid of this product has 50 levels (ranging from 0 to 5500 m), with a resolution of 1 m near the sea surface and 400 m into the deep ocean (Lamouroux et al., 2019). Such chl-a concentration profiles have shown good agreement with

150   both satellite and in situ measurements. Moreover, the depth of the deep chlorophyll maximum (DCM) is quite accurately simulated for the North Atlantic subtropical gyre (Lamouroux et al., 2019).

2.4.2   Drivers of ocean cooling

Post-storm SST cooling is a very complex process, involving hydrodynamic (vertical mixing and upwelling) and thermodynamic (surface heat flux) processes (Vincent et al., 2012a). Taking into account that cooling as a consequence of surface heat

155   loss is more relevant towards the shallow waters of the continental shelf (Morey et al., 2006; Ezer, 2018; Wei et al., 2018), we assessed the variability of the mixed layer and the thermocline displacement induced by Dorian and Humberto in order to identify the drivers of the post-storm-induced cooling. The mixed layer depth (MLD) data were derived from the Global Ocean Physics Analysis and Forecasting product distributed by CMEMS. MLD is defined by sigma theta considering a variable threshold criterion (equivalent to a 0.2 °C decrease), i.e., the depth where the density increase compared to density at 10 m

160   depth corresponds to a temperature decrease of 0.2 °C in local surface conditions (Chune et al., 2019).

   Upwelling and downwelling regimes can be identified by analysing the fluctuations in 20 °C isotherm depth (D20) (Jaimes and Shay, 2009, 2015), since D20 generally occurs within the area of maximum vertical temperature gradient in the tropical ocean. Therefore, D20 is considered as a proxy for the thermocline (Delcroix, 1984; Reverdin et al., 1986; Seager et al., 2019). The subtropical western Sargasso Sea has a particular vertical structure of its water column with a permanent thermocline at

165   approximately 400–500 m depth (Hill, 2005) and a seasonal thermocline in the upper ocean in summer (Hatcher and Battey, 2011). Between the seasonal and permanent thermocline, there is a layer with relatively homogeneous conditions, known as the western North Atlantic subtropical mode (STMW) water or 18-degree water because of its typical temperature (Schroeder et al., 1959; Kwon and Riser, 2004; Stevens et al., 2020). This layer is often defined by a temperature range of 17–19 °C (Billheimer and Talley, 2016), though a recent study used a broader range (16–20 °C) in order to account for mesoscale variability and

170   recent warming of STMW (Stevens et al., 2020). Consequently, we consider that the analysis of the upwelling response in terms of fluctuations in D20 will give insights into the vertical displacement of cool waters from the boundary of the seasonal thermocline and the STMW layer. We inferred daily D20 data from the SMARTS Climatology. D20 estimates have shown low RMSD value (RMSD≈0.2) during hurricane seasons in the western Sargasso Sea (see Figure 2-16 in Shay et al., 2019).

   Given the heterogeneous nature of the datasets used in this study, i.e., satellite and modelled data obtained using different

175   methods at different spatial resolutions, we focus on highlighting general spatio-temporal patterns of the analysed variables, since some specific dynamics may be a consequence of this heterogeneity.

3 Results

3.1 Physical response

3.1.1 Ocean cooling

180 During the pre-storm week of Dorian, the spatially averaged SST values along its trajectory and in the square study area were
29.6 and 29.4 °C, respectively, which were high compared to climatological records for the period 1982–2018, i.e., 29.02 and
28.73 °C, respectively. This points to a weak thermal contrast between the Gulf Stream Current and the adjacent waters to
its right (Figure 2A). Then, after the passage of Dorian, a considerable surface cooling was observed to the right side of its
trajectory during the first and second post-storm weeks (Figure 2B and C). During the pre-storm week of Dorian, TC Erin

185 affected the northerwestern Sargasso Sea (Blake, 2019) leading to a moderate SST cooling in the first post-storm week of
Dorian (Figure 2A and B). Then, after the passage of Humberto at the end of the second post-storm week, an intensive surface
cooling was observed in the entire area (Figure 2D and E).

For what concerns the daily evolution of SST anomalies we found that both along the trajectory and in the square study
area, SST started to decrease 3 days before Dorian's arrival reaching a maximum cooling of approximately 1 °C 1 to 3 days

190 after its passage (Figure 3A). The storm-induced subsurface thermal variability (described by OHC and T_{100}) changed in
phase with SST (Figure 3) though OHC and T_{100} differed significantly (Mann-Whitney test, $p < 0.05$) between the studied
areas (Figure 3B and C). More specifically, OHC and T_{100} values were 11 and 2% smaller (more negative) along Dorian's
trajectory as compared with the square study area during the first post-storm week (Figure 3B and C). Then, during the third
and fourth post-storm weeks SST, OHC and T_{100} decreased, with the lowest anomalies in the square study area (Figure 3). In

195 general, SST, OHC and T_{100} anomalies were then 34, 28 and 42% lower in this area than along Dorian's trajectory. Furthermore,
we found that during the first/second and third/fourth post-storm weeks 45 and 90% of SST anomalies in the square study area
accounted for a surface cooling of more than 1 °C, respectively, while 4 and 47% of SST anomalies accounted for a surface
cooling of more than 2 °C, respectively (Figure 4). Overall, SST, OHC and T_{100} anomalies in the square study area were 50,
63 and 57% lower in the third/fourth post-storm weeks than in the first/second post-storm weeks, respectively.

200 #### 3.1.2 Drivers of ocean cooling

We found fluctuations of the MLD before, during and after the passage of Dorian with no significant differences between the
studied areas when analysing the entire post-storm period (Mann-Whitney test, $p > 0.05$). The mixed layer started to deepen 3
days before Dorian's arrival in both study areas, reaching a maximum mean deepening of 10 and 11 m along Dorian's trajectory
and in the square study area at day 1 and 2, respectively (Figure 5A). A second maximum deepening was observed at the end

205 of the second post-storm week and the beginning of the third one (Figure 5A). On the other hand, D20 fluctuated consider-
ably during the analysed post-storm period, with significantly different values between the studied areas (Mann-Whitney test,
$p < 0.05$). The largest upward displacement of D20 during the first two post-storm weeks along the trajectory (Figure 5B) was
determined by the majority of pixels accounting for shoaling of this isotherm (61 and 56% of pixels along the trajectory and in
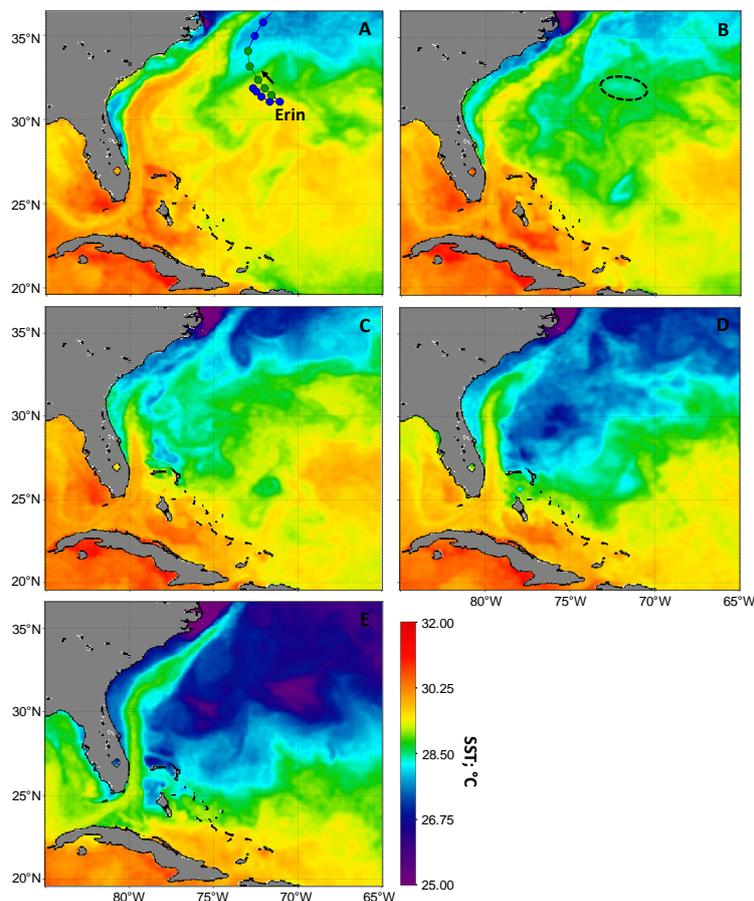
Figure 2. Weekly mean sea surface temperature (SST) in the (A) pre-storm week and (B) first, (C) second, (D) third and (E) fourth post-storm weeks of Dorian in the Sargasso Sea. Superimposed on (A) the trajectory of TC Erin, with colour coding as defined in Figure 1A and arrow indicating the direction of Erin's movement. The dashed contour in (B) indicates the surface cooling induced by Erin.

the square area, respectively, Figure 5C) since in both areas the net displacement of D20 was similar at this time (Figure 5D).

210 This spatial pattern changed during the third and fourth post-storm weeks, with a higher upward displacement of D20 in the square study area (Figure 5B), resulting from both the majority of pixels accounting for shoaling of this isotherm (60 and 73% of pixels along the trajectory and in the square area, respectively, Figure 5C) and a higher net displacement of D20 in those pixels (40 and 45 m along the trajectory and in the square, respectively, Figure 5D).

3.1.3 Climatological analysis of sea surface temperature

215 In order to assess the magnitude of the physical and biological response induced by Dorian and Humberto, we compared the mean SST and chl-a concentration during the third and fourth post-storm weeks of Dorian with the climatological records. Weekly and corresponding long-term arithmetic means (i.e., climatologies) were computed for each variable within the square
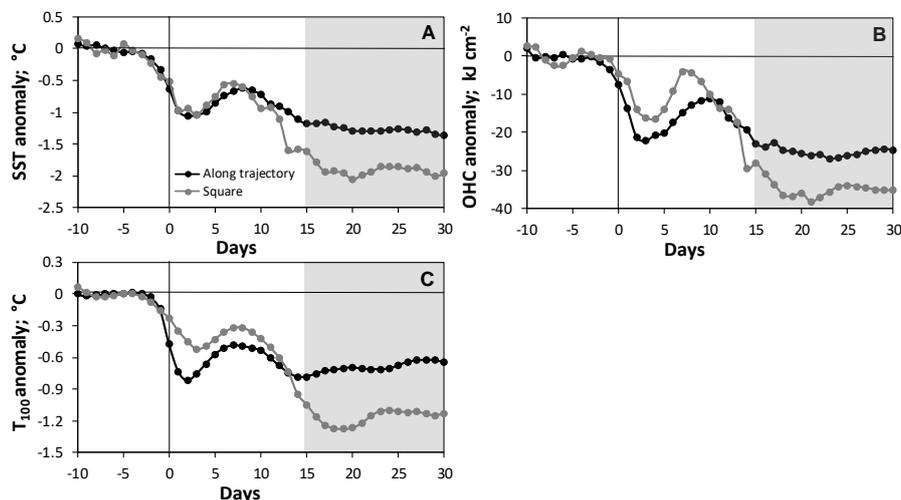
Figure 3. Daily mean evolution of anomalies of (A) sea surface temperature (SST), (B) ocean heat content (OHC) and (C) average temperature from the sea surface to a depth of 100 m (T_{100}) in the Sargasso Sea before, during and after the passage of Dorian and Humberto. The grey shaded area depicts the third and fourth post-storm weeks of Dorian which account for the combined effects of Dorian and Humberto.
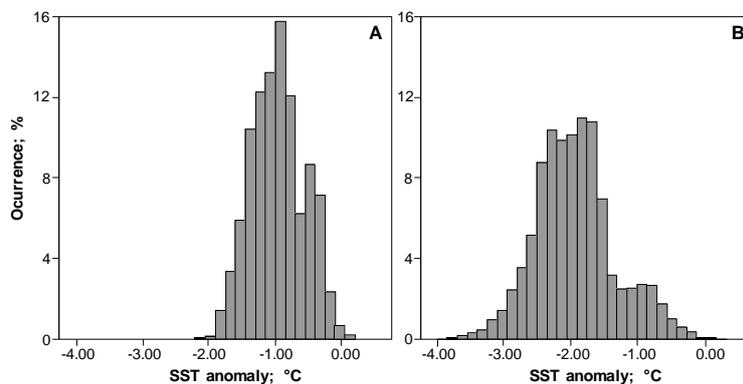
Figure 4. Sea surface temperature (SST) anomalies in the (A) first/second and (B) third/fourth post-storm weeks of Dorian in the square study area shown in Figure 1B.

study area for the period for which satellite observations were available, i.e., 1982–2018 for SST and 1998–2018 for chl-a concentration. We calculated standardized anomalies (deviations from the climatological weekly mean) by subtracting the
220 long-term weekly mean from the weekly mean of each variable. From Figure 6A we can see that the SST anomaly in the third post-storm week of Dorian was the most negative one in the last 14 years, while only 18% of anomalies where lower than the 2019 anomaly. On the other hand, the SST anomaly in the fourth post-storm week was the most negative one in the last 20 years, while only 13% of anomalies where lower than the one in 2019 (Figure 6A). In general, SST values in the square
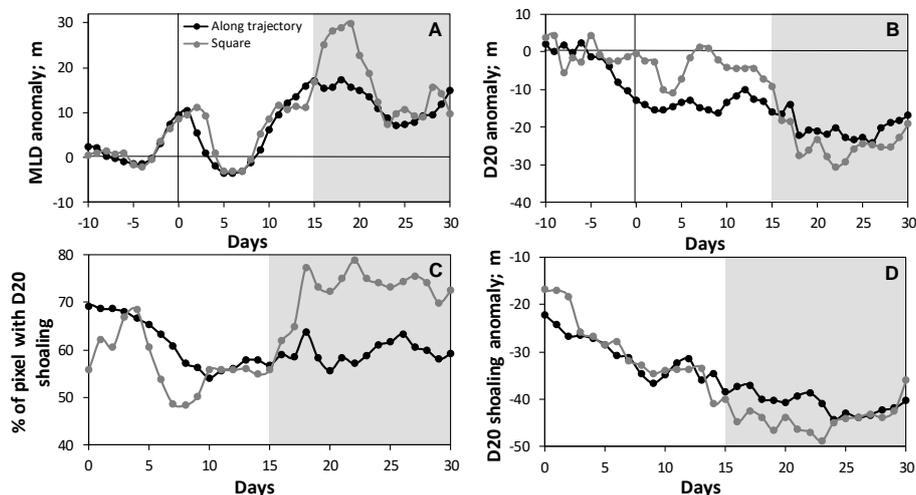
Figure 5. Daily mean evolution of anomalies of (A) mixed layer depth (MLD) and (B) 20 °C isotherm depth (D20) before, during and after the passage of Dorian and Humberto in the Sargasso Sea. (C) Percentage of pixels within each study area indicating upwelling in the post-storm period. From those pixels with upwelling, (D) displays the magnitude of the upward displacement of D20 as a measure of the seasonal thermocline upwelling. The grey shaded area depicts the third and fourth post-storm weeks of Dorian which account for the combined effects of Dorian and Humberto.

study area in the third and fourth post-storm weeks were significantly lower (Mann-Whitney test, $p <$) than the climatological

225 values at this time (Figure 7A). When assessing the SST response induced by Dorian and Humberto in a spatially explicit way, we observed that, indeed, these TCs led to a substantial SST cooling over the western Sargasso Sea (Figure 6B and C).

3.2 Biological response

3.2.1 Chlorophyll-a concentration bloom

During the pre-storm week of Dorian, the spatially averaged chl-a concentration along its trajectory and in the square study area

230 were 0.074 and 0.049 mg m^{-3}, respectively, which were low compared to climatological records for the period 1998–2018, i.e., 0.088 and 0.060 mg m^{-3}, respectively. Overall, chl-a concentration was low and spatially homogeneous in the deep waters of the western Sargasso Sea at this time, being quite distinct from the high-chl-a band along the east coast of USA (delineated by the 0.1 mg m^{-3} contour in Figure 8A). Then, following the passage of Dorian, we observed an oceanic chl-a increase and also an expansion of the coastal high-chl-a band during the entire post-storm period (Figure 8B–E). The oceanic biological

235 response was strongest in the waters to the north and northeast of Grand Bahama Island, especially during the third and fourth post-storm weeks (Figure 8D and E).

Taking into account the daily evolution of chl-a concentration anomalies we found that chl-a started to increase 3 days before Dorian's arrival (only along its trajectory, Figure 9A). Then, chl-a peaked at days 2 and 3 along its trajectory and in
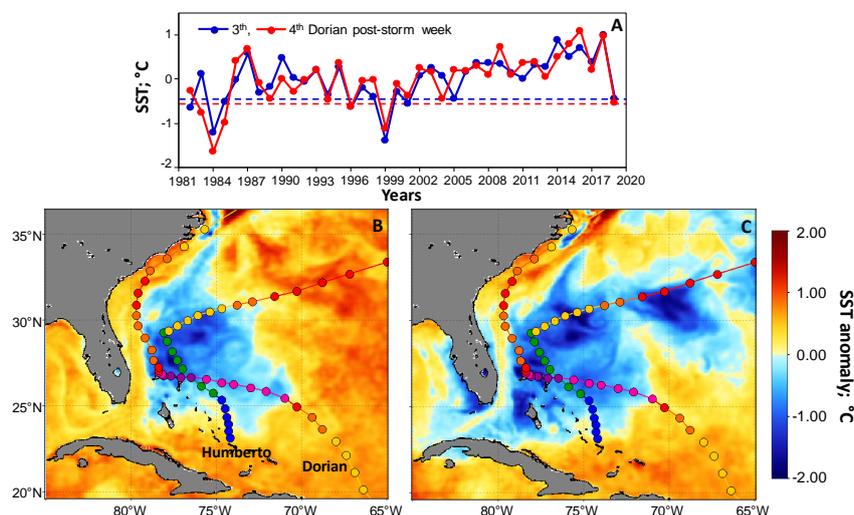
Figure 6. (A) Time series of weekly mean sea surface temperature (SST) anomalies during the third and fourth post-storm weeks of Dorian in the square study area shown in Figure 1B. The dashed lines mark anomalies in September 2019 for comparison with the previous years. (B) and (C) Spatially explicit SST anomalies (Dorian+Humberto induced effects – Climatology (1982–2018)) in the third and fourth post-storm weeks of Dorian, respectively.
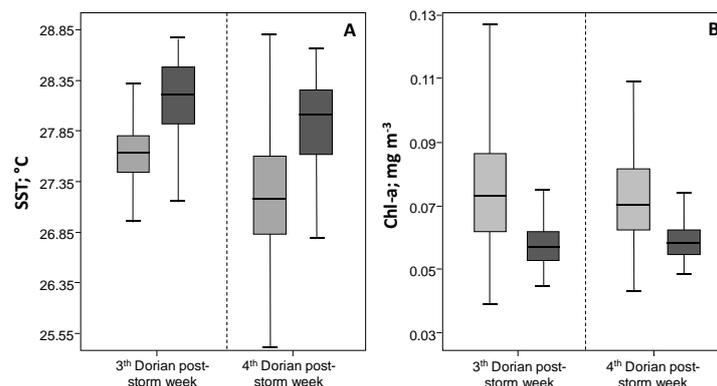
Figure 7. Dorian and Humberto induced (A) sea surface temperature (SST) and (B) chlorophyll-a (chl-a) concentration variability (light gray) with climatological records (dark grey) during the third and fourth post-storm week of Dorian in the square study area shown in Figure 1B.

the square study area, respectively, with anomalies being 23% higher in the former area than in the latter one during the first
240   two post-storm weeks. A second chl-a maximum was observed at the end of the second post-storm week along the trajectory, while in the square study area, chl-a concentration fluctuated considerably from the end of the second post-storm week on but still showing higher anomalies than the ones along the trajectory at this time (Figure 9A). When analysing the frequency of occurrence of chl-a concentration anomalies in the square study area during the first/second and third/fourth post-storm
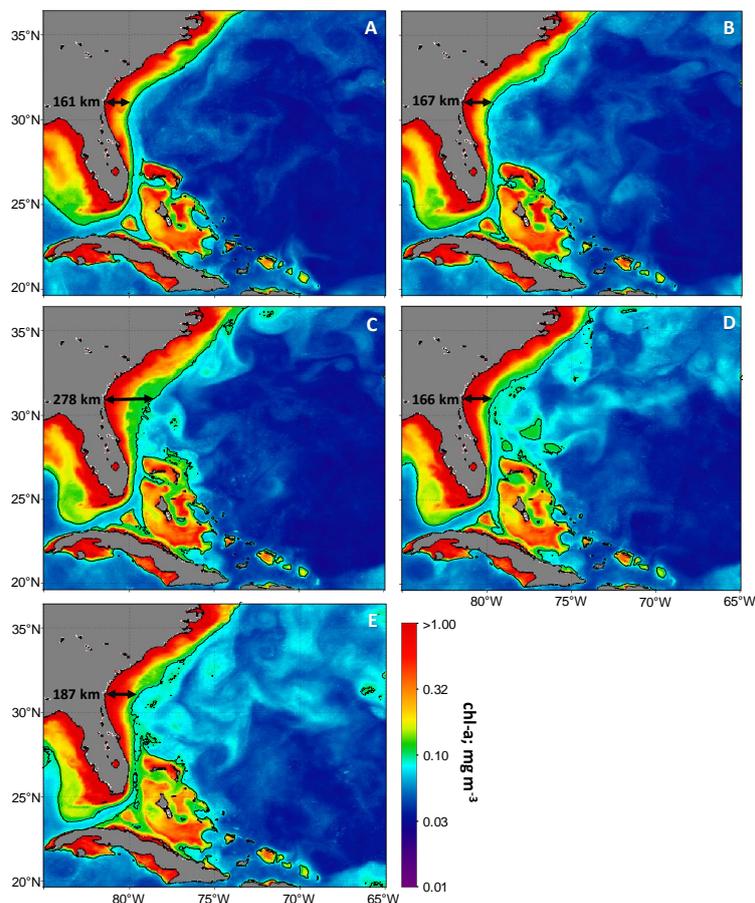
Figure 8. Weekly mean chlorophyll-a (chl-a) concentration in the (A) pre-storm week and (B) first, (C) second, (D) third and (E) fourth post-storm weeks of Dorian in the Sargasso Sea. The contour lines delineate chl-a concentration values 0.1 mg m^{-3} apart. Arrows indicate the distance from the coast to the 0.1 mg m^{-3} chl-a contour.

weeks, we found that 55 and 80% of the anomalies were higher than 0.01 mg m^{-3}, respectively, while, 36 and 57% of the

245   anomalies were higher than 0.02 mg m^{-3}, respectively (Figure 9B and C). Overall, surface chl-a concentration anomalies were 16% higher in the third/fourth post-storm weeks than in the first/second post-storm weeks in this area.

     In order to assess the subsurface biological response, we analysed vertical profiles of chl-a concentration in the square study area and in semi-disks 1 and 2 (see Figure 1B) given the high post-storm spatial variability of chl-a concentration profiles along Dorian's trajectory. Semi-disk 1 was crossed by both studied TCs, while semi-disk 2 was only affected by Dorian.

250   Although the DCM does not always coincide with biomass or productivity maxima, it often corresponds to peaks in abundance of phytoplankton (reviewed by Moeller et al., 2019). Thus, we considered the chl-a concentration in the DCM (chl-a$_{DCM}$) as a proxy of phytoplankton abundance.
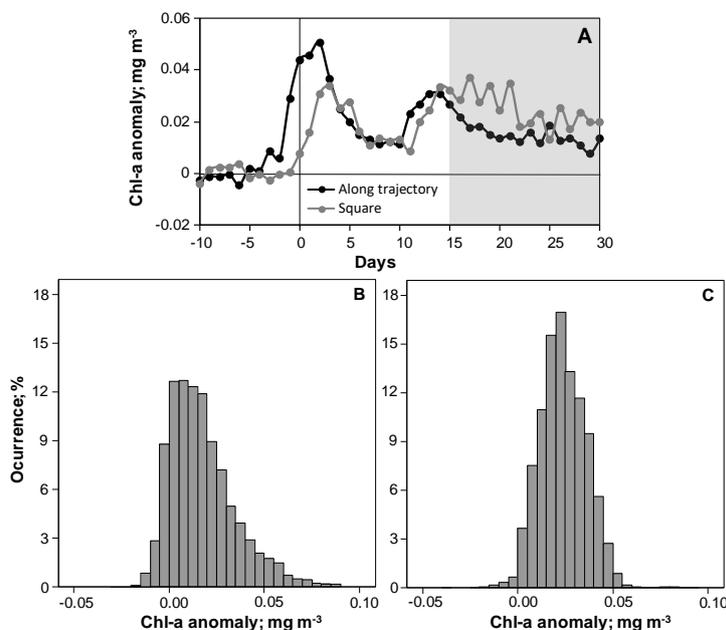
Figure 9. Daily mean evolution of (A) chlorophyll-a (chl-a) concentration anomalies in the western Sargasso Sea before, during and after the passage of Dorian and Humberto. The grey shaded area depicts the third and fourth post-storm weeks of Dorian which account for the combined effects of Dorian and Humberto. Distributions of chl-a concentration anomalies in the (B) first/second and (C) third/fourth post-storm weeks of Dorian in the square area delineated in Figure 1B.

Figure 10A shows that although the depth of the DCM (DCM_Z) did not change in the post-storm period, the mean chl-a concentration in the euphotic zone (chl-a$_{200}$) and chl-a$_{DCM}$ were 4 and 16% higher in the third/fourth post-storm weeks than in the first/second post-storm weeks, respectively (Figure 10A and Table 1). Besides, the chl-a profiles in semi-disk 1 showed the highest post-storm variability (Figure 10B). In this area, chl-a$_{200}$ and chl-a$_{DCM}$ were 9 and 16% higher in the third/fourth post-storm weeks than in the first post-storm week, respectively (Table 1). Moreover, DCM_Z was shallower in most post-storm weeks as compared to the pre-storm week (Figure 10B and Table 1), while in the second post-storm week the DCM could not be discerned (Figure 10B). Overall, the strong biological response in the third/fourth post-storm weeks as compared to the first/second post-storm weeks in these two areas is consistent with the maximum deepening of the MLD and shoaling of D20 (Figure 10A and B and Table 1). In contrast, the chl-a profiles in semi-disk 2 evolved differently (Figure 10C) with chl-a$_{200}$ being 25% lower in the third/fourth post-storm weeks than in the first/second post-storm weeks (Figure 10C and Table 1).

3.2.2 Climatological analysis of surface chlorophyll-a concentration

From Figure 11A we can infer that the mean chl-a concentration anomaly in the third post-storm week of Dorian in 2019 was the highest one in the last 9 years, while only 23% of anomalies were higher than the one in 2019. On the other hand, the chl-a concentration anomaly in the fourth post-storm week in 2019 was only surpassed by the one in 1999 (Figure 11A). In general,
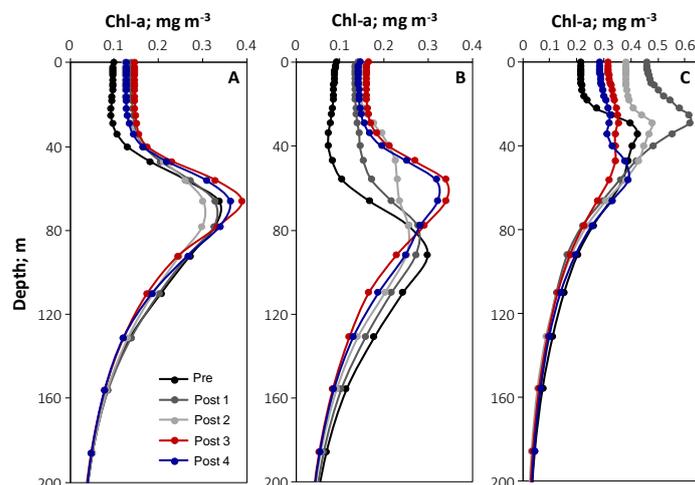
Figure 10. Spatially averaged chlorophyll-a (chl-a) concentration profiles in the (A) square study area and the 200 km radius semi-disks (B) 1 and (C) 2 shown in Figure 1B.

the chl-a concentration increase induced by the combined effect of Dorian and Humberto in the square area was significantly higher (Mann-Whitney test, $p < 0.05$) than climatological records (Figure 7B). In agreement with the spatial distribution of the most negative anomalies of SST shown in Figure 6B, the most positive chl-a anomalies during the third post-storm week

270   were observed to the north and northeast of Grand Bahama Island (Figure 11B) affected by the eyewall winds of these TCs. Conversely, in the fourth post-storm week positive chl-a anomalies (and negative SST anomalies in Figure 11C) were more evenly spread although, in general, a considerable response occurred in the latitudinal band 25–30 °N (Figure 11C).

4   Discussion

4.1   Ocean cooling and its drivers

275   The extensive surface cooling to the right of Dorian's trajectory (Figure 2B and C) agrees with the findings of Ezer (2018) for the Hurricane Matthew (2016), who followed a similar trajectory. This extensive cooling resulted from the interaction between a hurricane and the core of the Gulf Stream flow and its associated eddy field (Ezer, 2018). Figure 12A shows that, in some cases, maximum surface cooling occurred over areas with low values of sea surface height anomaly (SSHA) and oceanic cyclonic circulation, which correspond to cold-core eddies (Figure 12C). More specifically, the extensive cooling

280   observed in the center of the basin in Figure 12A largely agrees with the low SSHA values in it (Figure 12C). Owing to the special thermodynamic structure of cold-core eddies, the MLD within them is relatively shallower than in the adjacent ocean, which enhances the uplifting of cold and nutrient (chl-a-)rich subsurface waters by TC-induced vertical mixing (Ning et al.,

Table 1. Mean chlorophyll-a concentration in the euphotic zone (chl-a$_{200}$, mg m^{-3}), chl-a concentration at the deep chlorophyll maximum (chl-a$_{DCM}$, mg m^{-3}), depth of the DCM (DCM$_Z$, m), mixed layer depth (MLD, m) and 20 °C isotherm (D20, m) in the square study area, and semi-disks 1 and 2 shown in Figure 1B during the pre- and post-storm weeks of Dorian.

	Pre	Post 1	Post 2	Post 3	Post 4
Square					
chl-a$_{200}$	0.132	0.159	0.149	0.167	0.155
chl-a$_{DCM}$	0.338	0.328	0.301	0.389	0.362
DCM$_Z$	66	66	66	66	66
MLD	14	18	23	36	25
D20	198	193	193	172	173
Semi-disk 1					
chl-a$_{200}$	0.111	0.148	0.161	0.175	0.164
chl-a$_{DCM}$	0.299	0.276	-	0.339	0.319
DCM$_Z$	92	78	-	56	56
MLD	15	20	21	32	27
D20	253	223	225	209	211
Semi-disk 2					
chl-a$_{200}$	0.237	0.386	0.322	0.270	0.260
chl-a$_{DCM}$	0.426	0.618	0.479	-	0.390
DCM$_Z$	34	29	29	-	56
MLD	20	17	33	27	30
D20	180	185	177	189	209

2019). This also explains the increased chl-a concentration to the right of Dorian's trajectory in regions with oceanic cyclonic circulation (Figure 12B and C).

285   The retrieved temporal dynamics of the MLD during the first two post-storms weeks (Figure 5A) largely agrees with the one reported by Foltz et al. (2015). These authors found that during and immediately following a cyclone's passage, the spatially averaged MLD in the Sargasso Sea increases sharply by 7 m on average, while the positive anomaly rapidly diminishes during the subsequent days. Then, after the post-storm shoaling of the MLD, it can oscillate (shoaling/deepening) around the same mean depth (Foltz et al., 2015; Zhang et al., 2016; Prakash et al., 2018). However, this temporal evolution considers the oceanic

290   response to an individual TC. The second maximum deepening observed in our study at the beginning of the third post-storm week (Figure 5A) agrees with the suggestion made by Ezer et al. (2017), stating that several storms affecting the same region within a relatively short period of time have a cumulative impact on ocean mixing.

The fact that SST anomalies in both study areas are similar until day 11 (Figure 3A) follows for the fact that the center of Dorian moved over the warm waters of the Gulf Stream current. Despite the Dorian-induced SST decrease in the area, still

295   the warm core of the Gulf Stream was observed most post-storm days (e.g., Figures 2B and 12A). On the other hand, it has
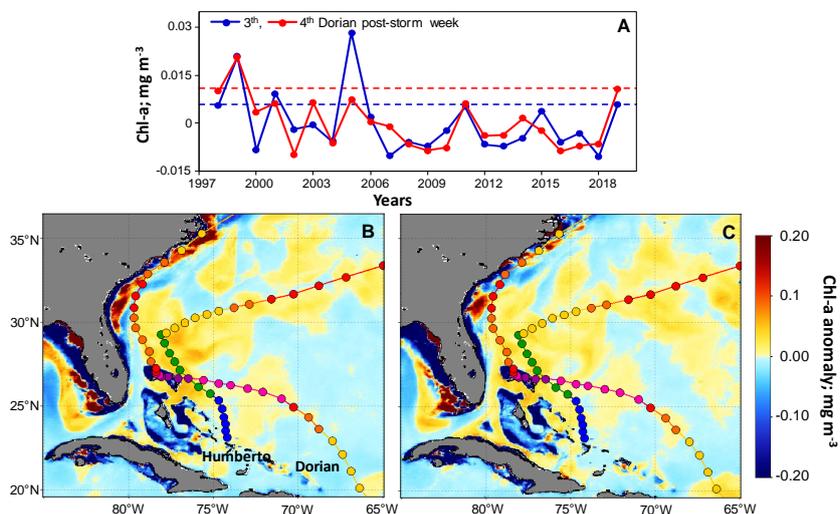
Figure 11. (A) Time series of weekly mean chlorophyll-a (chl-a) concentration anomalies during the third and fourth post-storm weeks of Dorian in the square study area delineated in Figure 1B. The dashed lines mark anomalies in September 2019 for comparison with the previous years. (B) and (C) Spatially explicit chl-a anomalies (Dorian+Humberto induced effects – Climatology (1998–2018)) in the third and fourth post-storm weeks of Dorian, respectively.

been reported that sea surface cooling induced by TCs can extend over vast areas far from the area affected by the TC center because of the remotely-induced mixing (Oey et al., 2006, 2007; Vincent et al., 2012a; Menkes et al., 2016; Ezer, 2018). This contributed to the SST decrease in the square study area and the deepening of the mixed layer 3 days before the arrival of Dorian in both study areas (Figures 3A and 5A). Summer conditions in the Sargasso Sea are characterized by a strong thermal
300 stratification of the upper water column leading to shallow mixed layers (< 20 m) (Michaels et al., 1993; Steinberg et al., 2001). Spatially averaged MLD during the pre-storm week were approximately 14 and 16 m along the trajectory and in the square study area, respectively. Shallow mixed layers indicate that there is cold water near the surface, so that wind-induced mixing generates immediate surface cooling. This agrees with the fact waters of the western Sargasso Sea have a low resistance to TC-induced cooling through mixing (see Figure 5b in Vincent et al., 2012b).
305   Overall, we consider that surface cooling was largely modulated by vertical mixing. Ezer (2018) reported that vertical mixing drove cooling of the upper 50 m after the passage of Matthew across the Sargasso Sea. In contrast, deep cooling is more sensitive to upwelling of the thermocline, which explains the more negative anomalies of OHC and T_{100} along the trajectory in the first two post-storm weeks and in the square study area during the last two post-weeks (Figure 3B and C). TCs typically give rise to upwelling flow underneath the storm centre and weak downwelling of the displaced warm water over a broad area
310 beyond the upwelled regions (Price, 1981; Jullien et al., 2012; Fu et al., 2014). Overall, TC-induced upwelling by Ekman pumping plays a major role in inducing cooling under the TC center (e.g., Jullien et al., 2012; Wei et al., 2018).
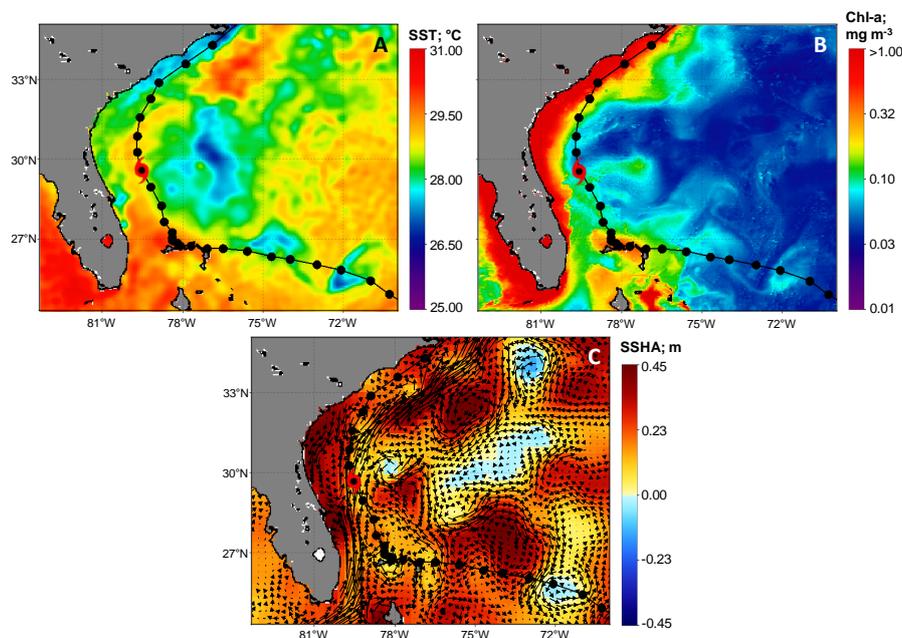
Figure 12. Oceanic response to Dorian (September 4, 2019). (A) Sea surface temperature (SST), (B) chlorophyll-a (chl-a) concentration and (C) sea surface height anomaly (SSHA) with geostrophic current vectors superimposed (data derived from Salto/DUACS gridded multimission altimeter at $0.25° \times 0.25°$ spatial resolution). The trajectory of Dorian and a hurricane symbol indicating its estimated position is superimposed in all imagines.

4.2 Chlorophyll-a concentration bloom

The increased post-storm chl-a_{200} and chl-a_{DCM}, as well as the upward displacement of the DCM (Figure 10 and Table 1), is consistent with previous observations in several oceanic basins around the world (e.g., Ye et al., 2013; Chacko, 2017; Chakraborty et al., 2018; Jayaram et al., 2019). A DCM typically occurs in stratified and oligotrophic marine environments where phytoplankton are not evenly distributed throughout the water column (Liccardo et al., 2013; Macías et al., 2013). In this case, the shape of the vertical profiles of chl-a concentration can be considered as Gaussian according to the classification of Mignot et al. (2011, 2014). In contrast, in environments with a deep and strong mixing, phytoplankton are homogeneously distributed in the mixed layer and chl-a profiles are sigmoid (Mignot et al., 2011, 2014). Given the TC-enhanced vertical mixing and deepening of the mixed layer, a shift from Gaussian to sigmoid-like shape of the chl-a profiles can be expected after the passage of TCs across a stratified area (Wu et al., 2007). However, a considerable post-storm change of chlorophyll in the surface mixed layer occurs when the MLD is deeper than the DCM (Wu et al., 2007), which explains the Gaussian-shaped profiles after the passage of Dorian and Humberto (Figure 10) since MLD was typically shallower than the DCM (Table 1).

On the other hand, the increased post-storm chl-a_{200} (Figure 10 and Table 1) indicates that subsurface phytoplankton bloom was due to new production resulting from a nutrient influx into the euphotic layer instead of a vertical chl-a redistribution.

This also explains the increased post-storm chl-a$_{DCM}$ as well as the shallower DCM$_Z$ (Figure 10 and Table 1). The formation and persistence of the DCM is governed by biophysical processes accounting for both bottom-up and top-down controls (Cullen, 2015; Moeller et al., 2019). However, given that light and nutrient availability are primary factors governing phytoplankton abundance and distribution, they have also been recognized as relevant drivers of phytoplankton communities

330   in the DCM (Latasa et al., 2016). It has been reported that turbulence (like the one induced by storms) can enlarge the phytoplankton density above the DCM (Liccardo et al., 2013) leading to a shoaling of the DCM. Given that the DCM occurs at the transition between the light-limited region (below the maximum) and nutrient-limited region (above the maximum), a limited addition of nutrients into the region immediately above the DCM, shifts the system from a nutrient-limited regime to a light-limited one (Liccardo et al., 2013).

335   Although strong mixing due to TCs is mostly confined to the upper ocean, the cyclone-induced inertial waves affect the subsurface mixing too (Prakash et al., 2018). Part of the energy transferred to inertial currents by the storm may propagate below the mixed layer and finally drive turbulent mixing in the thermocline (Cuypers et al., 2013). Given that wind-generated inertial waves can propagate up to 2000 m depth in the Sargasso Sea (Morozov and Velarde, 2008), this subsurface mixing can reach the DCM and nitracline and consequently transport chl-a and nutrients to the mixed layer (Foltz et al., 2015). The

340   nitracline depth in the northern Sargasso Sea in summer oscillates between 90–150 m (Malone et al., 1993; Goericke and Welschmeyer, 1998), though it decreases after the passage of TCs (Malone et al., 1993). So, the upward nutrient advection from the nitracline after the passage of TCs can fuel subsurface phytoplankton productivity.

  For what concerns the post-storm surface chl-a response, we argue that it was mainly determined by entrainment of chl-a from deep waters given the rapid increase of the surface chl-a concentration as soon as a TC reached the study areas, which

345   agrees with the suggestion of Shropshire et al. (2016). Figure 12B shows a patch of high chl-a concentration (0.13 mg m^{-3}) to the right of Dorian's trajectory the day it affected the area confirming the immediate biological response to the TC forcing. Although the mixed layer did not reach the DCM in the study area (Table 1), it is likely that a small amount of chl-a was eventually transported to the surface since deep near-inertial mixing can raise the surface chl-a concentration (Wang et al., 2020). The higher chl-a concentration anomalies along the trajectory as compared the ones in the square study area from day –

350   3 to 3 (Figure 9A) are associated with both an increased upward displacement of D20 (Figure 5B) and the horizontal advection of chl-a-rich waters from the coast of the northwestern Bahamas islands and the east coast of USA, which were impacted by Dorian (Avila et al., 2020). These higher chl-a concentration anomalies are consistent with the fact that surface phytoplankton blooms are common near the TC trajectory (e.g., Babin et al., 2004; Walker et al., 2005; Gierach and Subrahmanyam, 2008; Lin and Oey, 2016; Avila-Alonso et al., 2019).

355   **4.3   Climatological analysis of sea surface temperature and chlorophyll-a concentration**

TC activity in the North Atlantic basin peaks from late August to September (Neely, 2016). Thus, given that the third and fourth post-storm weeks of Dorian occurred in September, the time series of weekly mean anomalies of SST and chl-a concentration (Figures 6A and 11A) indicated the oceanic responses to preceding TCs. For instance, extreme anomalies observed in 1999 (Figures 6A and 11A) were associated with the passage of Hurricanes Dennis and Floyd at the end of August and

360   September of that year (Figure 13). These consecutive hurricanes were two weeks apart (Pasch et al., 1999; Beven, 2000) and induced a considerable oceanic response (Figure 13). Other extreme SST and chl-a concentration anomalies were the ones in 1984 and 2005 (Figures 6A and 11A) associated with Hurricanes Diana (1984) and Ophelia (2005). Both hurricanes followed peculiar trajectories since they made clockwise loops leading to a prolonged forcing time over the ocean and consequently to a strong oceanic response (Lawrence and Clark, 1985; Beven and Cobb, 2006).

365   The strong oceanic response to the combined effect of Dorian and Humberto was reinforced by the fact that they were slow-moving TCs. We computed the translation speed of Dorian and Humberto following the procedure outlined by Babin et al. (2004) and Gierach and Subrahmanyam (2008) using the "best track" observations of time and position from the HURDAT2 database of the National Hurricane Center (*http://www.aoml.noaa.gov/hrd/ hurdat/hurdat2.html*). In order to classify these TCs on the basis of their translation speed we followed the approach by Avila-Alonso et al. (2020), i.e., a fast (slow) moving TC

370 has a higher (lower) translation speed than the climatological one computed for Atlantic TCs averaged in 5-degree latitude bins (see table in *https://www.aoml.noaa.gov/hrd-faq/#tropical-cyclone-climatology*, consulted in May 2020). We found that Dorian and Humberto had a mean translation speed of 10.95 and 12.8 km h^{-1}, respectively, in the 25–30 °N latitudinal band, while the corresponding mean climatological translation speed is 20.1 km h^{-1}. This finding agrees with the decreasing TC translation speed observed at global scale in general, and in the North Atlantic basin in particular, as a consequence of

375 the global-warming-induced changes in global atmospheric circulation (Kossin, 2018). Although we acknowledge that pre-storm oceanographic conditions influence the magnitude of the induced-oceanic post-storm response (Nigam et al., 2019), our climatological analysis revealed that the strongest oceanographic response in the western Sargasso Sea is associated with consecutive TCs and long-lasting TC forcing.

   Climatological SST responses to the passage of TCs in all TC-prone regions around the world indicate that maximum

380 cooling occurs 2 days after the TC passage and then cooling starts decreasing from this day onward (Menkes et al., 2016). Moreover, although the TC-induced cold wake in the North Atlantic basin needs about 60 days to disappear, it decays (80%) in the first 20 days (Haakman et al., 2019). On the other hand, even though post-storm blooms can last about 2–3 weeks, their peak occurs following the passage of TCs (at days 3 to 4) (Menkes et al., 2016). However, we found that the passage of a second TC disrupts these global patterns leading to a decreasing SST trend and a second chl-a bloom. This finding agrees

385 with the one reported in Avila-Alonso et al. (2019) for the waters surrounding Cuba since they found a progressive post-storm surface cooling during a month after the passage of hurricanes, which was partially determined by the passage of consecutive hurricanes across the study area. Moreover, extensive and long-lasting SST cooling as well as intense post-storm phytoplankton blooms after the passage of consecutive TCs have been documented in the northwestern Pacific Ocean (e.g., Wu and Li, 2018; Ning et al., 2019; Wang et al., 2020). Overall, consecutive TCs superimpose effects on the upper ocean response because of

390 strong-induced mixing and upwelling (Wu and Li, 2018; Ning et al., 2019; Wang et al., 2020).

   The TC-induced oceanographic variability impacts marine trophic communities in general (e.g., Fiedler et al., 2013; Hung et al., 2014). Pedrosa-Pàmies et al. (2018) reported that Hurricane Nicole (2016) caused phytoplankton bloom and increased zooplankton and bacterial abundance in the deep water column in the Bermuda Time-Series Site in the Sargasso Sea, indicating a coupled post-storm response of primary and secondary production. The Sargasso Sea is the spawning area of the European
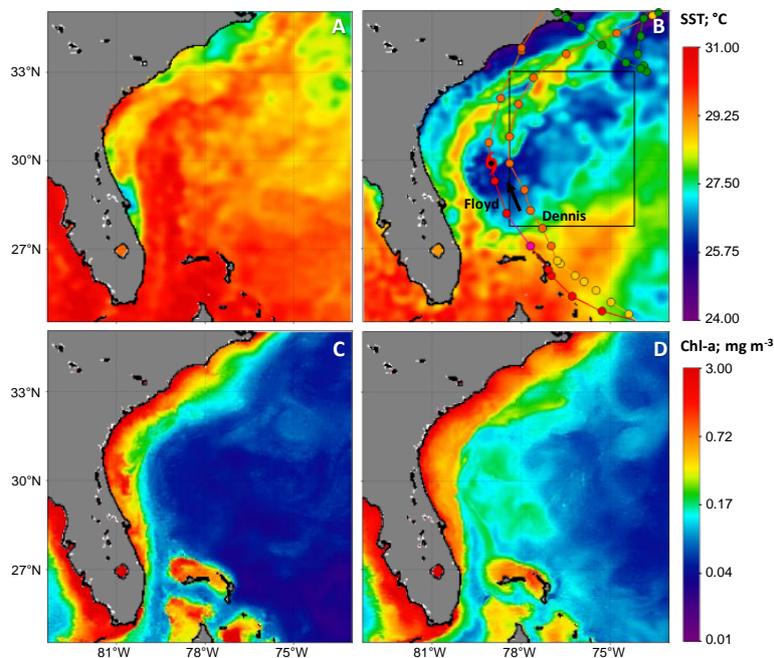
Figure 13. (A and B) Sea surface temperature (SST) and (C and D) chlorophyll-a (chl-a) concentration before (A and C, August 25, 1999) and after (B and D, September 15, 1999) the passage of Hurricanes Dennis and Floyd across the waters of the western Sargasso Sea. Superimposed in (B) the square study area and the trajectory of Dennis and Floyd, with colour coding as defined in Figure 1A. The arrow indicates the direction of the TCs movement and the hurricane symbol indicates the estimated position of Floyd.

395 and American eels (*Anguilla anguilla* Linnaeus 1758 and *A. rostrate* LeSueur, respectively) (Schmidt, 1923; van Ginneken and Maes, 2005; Friedland et al., 2007; Miller et al., 2019a). Spawning and retention of larvae are associated with relatively productive zones that may enhance feeding opportunities (Kleckner and McCleave, 1988; Munk et al., 2010). Eels survival during their early larvae stages is strongly correlated with food availability, specifically with planktonic organisms (Riemann et al., 2010; Ayala et al., 2018). Consequently, climate-driven processes affecting nutrient availability and phytoplankton primary

400 production affect levels of eel larval survival in areas with high spawning activity, as well as its recruitment (Bonhommeau et al., 2008a, b; Miller et al., 2016). Considering that the TC-induced chl-a concentration changes may impact the survival rates of fish larvae and their recruitment to adulthood in the Sargasso Sea (Foltz et al., 2015), the assessment of the oceanic response to TCs serves for future studies addressing the influence of climate variability on fishery oceanography in the region.

5   Conclusions

405 In this work, multi-platform datasets were used to investigate the physical and biological responses of the upper ocean to the consecutive Hurricanes Dorian and Humberto in the western Sargasso Sea. Dorian induced an extensive surface cooling to

the right side of its trajectory which was associated with the presence of cold-core eddies in the area. This extensive cooling was mainly driven by vertical mixing while the post-storm decreases of OHC and T_{100} were mostly governed by the upward displacement of D20. On the other hand, Dorian led to an increased chl-a concentration, which was 23% higher along the tra-

410   jectory than in the square study area during the first two post-storm weeks. This biological response is essentially determined by entrainment of chl-a from depth and horizontal advection of coastal productive waters. Then, at the end of the second post-storm week of Dorian, Humberto started to affect the study area superimposing effects on the upper ocean response because of the strong-induced mixing and upwelling. Overall, anomalies of SST, OHC and T_{100} were 50, 63 and 57% lower in the third/fourth post-storm weeks than in the first/second post-storm weeks of Dorian, respectively, while surface chl-a concentra-

415   tion anomalies, chl-a$_{200}$ and chl-a$_{DCM}$ were 16, 4 and 16% higher in the third/fourth post-storm weeks than in the first/second post-storm weeks, respectively. Furthermore, the combined effects of these TCs induced an upward displacement of the DCM in some analysed cases. This subsurface biological response indicates the stimulation of new production because of the upward nutrient fluxes. The surface SST and chl-a concentration responses induced by Dorian and Humberto were significantly more intense (Mann-Whitney test $p < 0.05$) as compared to climatological records. Our climatological analysis revealed that the

420   strongest TC-induced oceanographic variability in the western Sargasso Sea has been associated with consecutive TCs and long-lasting TC forcing.

Data availability. For satellite products presented in this work, please contact the corresponding author at davila@uclv.cu

Author contributions. All authors together have contributed to the research reported in different ways. D.A.-A., conceived and designed this study in general, conducted the collection, processing and analysis of data and wrote the original draft. J.M.B., contributed to methodological

425   aspects and to the design of the study, carefully reviewed and edited the English. R.C., assisted to the interpretation of results, and provided comments and suggestions on the paper. Revising it for important intellectual content. B.D.B carefully reviewed and edited the English. Provided comments and suggestions on the paper. Supervision and funding acquisition.

Competing interests. The authors declare that they have no known competing financial interests or personal relationships that could have appeared to influence the work reported in this paper.

430   *Acknowledgements.* This work was supported by the Special Research Fund (BOF) of Ghent University, Belgium, Grant Code 01W03715.

References

Augustyn, A., Bauer, P., Duignan, B., Eldridge, A., Gregersen, E., McKenna, A., Petruzzello, M., Rafferty, J., Ray, M., Rogers, K., Tikkanen, A., Wallenfeldt, J., Zeidan, A., , and Zelazko, A.: Sargasso Sea. Encyclopaedia Britannica, https://www.britannica.com/place/Sargasso-Sea (accessed April, 2020), 2013.

Avila, L. A., Stewart, S., Berg, R., and Hagen, A.: Tropical cyclone report Hurricane Dorian, 24 August–7 September, 2019, National Hurricane Center, https://www.nhc.noaa.gov/data/tcr, 2020.

Avila-Alonso, D., Baetens, J. M., Cardenas, R., and De Baets, B.: The impact of hurricanes on the oceanographic conditions in the Exclusive Economic Zone of Cuba, Remote Sensing of Environment, p. 111339, doi:10.1016/j.rse.2019.111339, 2019.

Avila-Alonso, D., Baetens, J. M., Cardenas, R., and De Baets, B.: Oceanic response to Hurricane Irma (2017) in the Exclusive Economic Zone of Cuba and the eastern Gulf of Mexico, Ocean Dynamics, 70, 603–619, doi:10.1007/s10236-020-01350-y, 2020.

Ayala, D. J., Munk, P., Lundgreen, R. B., Traving, S. J., Jaspers, C., Jørgensen, T. S., Hansen, L. H., and Riemann, L.: Gelatinous plankton is important in the diet of European eel (*Anguilla anguilla*) larvae in the Sargasso Sea, Scientific Reports, 8, 6156, doi:10.1038/s41598-018-24388-x, 2018.

Babin, S. M., Carton, J. A., Dickey, T. D., and Wiggert, J. D.: Satellite evidence of hurricane-induced phytoplankton blooms in an oceanic desert, Journal of Geophysical Research: Oceans, 109, C03 043, doi:10.1029/2003JC001938, 2004.

Bacmeister, J. T., Reed, K. A., Hannay, C., Lawrence, P., Bates, S., Truesdale, J. E., Rosenbloom, N., and Levy, M.: Projected changes in tropical cyclone activity under future warming scenarios using a high-resolution climate model, Climatic Change, 146, 547–560, 2018.

Bang, H., Miles, L., and Gordon, R.: Hurricane occurrence and seasonal activity: an analysis of the 2017 Atlantic hurricane season, American Journal of Climate Change, 8, 454–481, 2019.

Baranowski, D., Flatau, P., Chen, S., and Black, P.: Upper ocean response to the passage of two sequential typhoons, Ocean Science, 10, 559–570, 2014.

Beven, J.: Tropical cyclone preliminary report Hurricane Dennis, 24 August–7 September, 1999, National Hurricane Center, https://www.nhc.noaa.gov/data/tcr, 2000.

Beven, J. and Cobb, H.: Tropical cyclone report Hurricane Ophelia, 6–17 September 2005, National Hurricane Center, https://www.nhc.noaa.gov/data/tcr, 2006.

Bhatia, K., Vecchi, G., Murakami, H., Underwood, S., and Kossin, J.: Projected response of tropical cyclone intensity and intensification in a global climate model, Journal of Climate, 31, 8281–8303, 2018.

Bhatia, K. T., Vecchi, G. A., Knutson, T. R., Murakami, H., Kossin, J., Dixon, K. W., and Whitlock, C. E.: Recent increases in tropical cyclone intensification rates, Nature Communications, 10, 635, doi:10.1038/s41467-019-08471-z, 2019.

Billheimer, S. and Talley, L. D.: Annual cycle and destruction of Eighteen Degree Water, Journal of Geophysical Research: Oceans, 121, 6604–6617, 2016.

Blake, E. S.: Tropical cyclone report Tropical Storm Erin, 26–29 August 2019, National Hurricane Center, https://www.nhc.noaa.gov/data/tcr, 2019.

Bonhommeau, S., Chassot, E., Planque, B., Rivot, E., Knap, A. H., and Le Pape, O.: Impact of climate on eel populations of the Northern Hemisphere, Marine Ecology Progress Series, 373, 71–80, 2008a.

Bonhommeau, S., Chassot, E., and Rivot, E.: Fluctuations in European eel (*Anguilla anguilla*) recruitment resulting from environmental changes in the Sargasso Sea, Fisheries Oceanography, 17, 32–44, 2008b.

Camargo, S. J. and Wing, A. A.: Tropical cyclones in climate models, Wiley Interdisciplinary Reviews: Climate Change, 7, 211–237, 2016.

Chacko, N.: Chlorophyll bloom in response to tropical cyclone Hudhud in the Bay of Bengal: Bio-Argo subsurface observations, Deep Sea
470   Research Part I: Oceanographic Research Papers, 124, 66–72, 2017.

Chakraborty, K., Nimit, K., Akhand, A., Prakash, S., Paul, A., Ghosh, J., Bhaskar, T. U., and Chanda, A.: Modeling the enhancement of sea
surface chlorophyll concentration during the cyclonic events in the Arabian Sea, Journal of Sea Research, 140, 22–31, 2018.

Cheng, L., Zhu, J., Abraham, J., Trenberth, K. E., Fasullo, J. T., Zhang, B., Yu, F., Wan, L., Chen, X., and Song, X.: 2018 continues record
global ocean warming, Advances in Atmospheric Sciences, 36, 249–252, 2019.

475 Chih, C.-H. and Wu, C.-C.: Exploratory analysis of upper-ocean heat content and sea surface temperature underlying tropical cyclone rapid
intensification in the western North Pacific, Journal of Climate, 33, 1031–1050, 2020.

Chune, S., Nouel, L., Fernandez, E., Derval, C., and Tressol, M.: Product user manual for the Global Ocean Sea Physical Analysis and Fore-
casting products, Issue: 1.5. Copernicus Marine Environment Monitoring Service, http://marine.copernicus.eu/documents/PUM/CMEMS-
GLO-PUM-001-024.pdf, 2019.

480 Cullen, J. J.: Subsurface chlorophyll maximum layers: enduring enigma or mystery solved?, Annual Review of Marine Science, 7, 207–239,
2015.

Cuypers, Y., Le Vaillant, X., Bouruet-Aubertot, P., Vialard, J., and Mcphaden, M. J.: Tropical storm-induced near-inertial internal waves
during the Cirene experiment: energy fluxes and impact on vertical mixing, Journal of Geophysical Research: Oceans, 118, 358–380,
2013.

485 Davis, A. and Yan, X.-H.: Hurricane forcing on chlorophyll-a concentration off the northeast coast of the US, Geophysical Research Letters,
31, L17 304, doi:10.1029/2004GL020668, 2004.

de Beurs, K. M., McThompson, N. S., Owsley, B. C., and Henebry, G. M.: Hurricane damage detection on four major Caribbean islands,
Remote Sensing of Environment, 229, 1–13, doi:10.1016/j.rse.2019.04.028, 2019.

Deacon, G.: The Sargasso Sea, The Geographical Journal, 99, 16–28, 1942.

490 Defforge, C. L. and Merlis, T. M.: Observed warming trend in sea surface temperature at tropical cyclone genesis, Geophysical Research
Letters, 44, 1034–1040, 2017.

Delcroix, T.: EOF analysis of the thermocline depth in the tropical Atlantic Ocean, Tropical Ocean Atmosphere Newsletter, 27, 18–19, 1984.

Deo, A., Ganer, D., and Nair, G.: Tropical cyclone activity in global warming scenario, Natural Hazards, 59, 771–786, 2011.

Donlon, C. J., Martin, M., Stark, J., Roberts-Jones, J., Fiedler, E., and Wimmer, W.: The operational sea surface temperature and sea ice
495   analysis (OSTIA) system, Remote Sensing of Environment, 116, 140–158, 2012.

Ezer, T.: On the interaction between a hurricane, the Gulf Stream and coastal sea level, Ocean Dynamics, 68, 1259–1272, 2018.

Ezer, T., Atkinson, L. P., and Tuleya, R.: Observations and operational model simulations reveal the impact of Hurricane Matthew (2016) on
the Gulf Stream and coastal sea level, Dynamics of Atmospheres and Oceans, 80, 124–138, 2017.

Farfán, L. M., D'Sa, E. J., Liu, K.-b., and Rivera-Monroy, V. H.: Tropical cyclone impacts on coastal regions: the case of the Yucatán and the
500   Baja California Peninsulas, Mexico, Estuaries and Coasts, 37, 1388–1402, 2014.

Fiedler, P. C., Redfern, J. V., Van Noord, J., Hall, C., Pitman, R. L., and Ballance, L. T.: Effects of a tropical cyclone on a pelagic ecosystem
from the physical environment to top predators, Marine Ecology Progress Series, 484, 1–16, doi:10.3354/meps10378, 2013.

Foltz, G. R., Balaguru, K., and Leung, L. R.: A reassessment of the integrated impact of tropical cyclones on surface chlorophyll in the
western subtropical North Atlantic, Geophysical Research Letters, 42, 1158–1164, 2015.

505   Friedland, K. D., Miller, M. J., and Knights, B.: Oceanic changes in the Sargasso Sea and declines in recruitment of the European eel, ICES
        Journal of Marine Science, 64, 519–530, 2007.

Fu, H., Wang, X., Chu, P. C., Zhang, X., Han, G., and Li, W.: Tropical cyclone footprint in the ocean mixed layer observed by Argo in the
        Northwest Pacific, Journal of Geophysical Research: Oceans, 119, 8078–8092, 2014.

Garnesson, P., Mangin, A., and Bretagnon, M.:   Ocean colour production centre. Satellite Observation. GlobColour-
510   Copernicus Products. Quality information document , Copernicus Marine Environment Monitoring Service. 82 pp.
        http://marine.copernicus.eu/documents/QUID/CMEMS-OC-QUID-009-030-032-033-037-081-082-083-085-086-098.pdf, 2019a.

Garnesson, P., Mangin, A., d'Andon, O. F., Demaria, J., and Bretagnon, M.: The CMEMS GlobColour chlorophyll a product based on
        satellite observation: multi-sensor merging and flagging strategies, Ocean Science, 15, 819–830, 2019b.

Gierach, M. M. and Subrahmanyam, B.: Biophysical responses of the upper ocean to major Gulf of Mexico hurricanes in 2005, Journal of
515   Geophysical Research: Oceans, 113, C04 029, doi:10.1029/2007JC004419, 2008.

Goericke, R. and Welschmeyer, N. A.: Response of Sargasso Sea phytoplankton biomass, growth rates and primary production to seasonally
        varying physical forcing, Journal of Plankton Research, 20, 2223–2249, 1998.

Gohin, F.: Annual cycles of chlorophyll-a, non-algal suspended particulate matter, and turbidity observed from space and in-situ in coastal
        waters, Ocean Science, 7, 705–732, 2011.

520   Gohin, F., Druon, J., and Lampert, L.: A five channel chlorophyll concentration algorithm applied to SeaWiFS data processed by SeaDAS in
        coastal waters, International Journal of Remote Sensing, 23, 1639–1661, 2002.

Haakman, K., Sayol, J.-M., van der Boog, C. G., and Katsman, C. A.: Statistical characterization of the observed cold wake induced by North
        Atlantic hurricanes, Remote Sensing, 11, 2368, doi:10.3390/rs11202368, 2019.

Hanshaw, M. N., Lozier, M. S., and Palter, J. B.: Integrated impact of tropical cyclones on sea surface chlorophyll in the North Atlantic,
525   Geophysical Research Letters, 35, doi:10.1029/2007GL031862, 2008.

Hatcher, P. E. and Battey, N.: Biological diversity: exploiters and exploited, John Wiley & Sons, USA, 2011.

Henderson-Sellers, A., Zhang, H., Berz, G., Emanuel, K., Gray, W., Landsea, C., Holland, G., Lighthill, J., Shieh, S.-L., Webster, P., et al.:
        Tropical cyclones and global climate change: a post-IPCC assessment, Bulletin of the American Meteorological Society, 79, 19–38, 1998.

Hernández, W. J., Ortiz-Rosa, S., Armstrong, R. A., Geiger, E. F., Eakin, C. M., and Warner, R. A.: Quantifying the effects of Hurri-
530   canes Irma and Maria on coastal water quality in Puerto Rico using Moderate Resolution Satellite Sensors, Remote Sensing, 12, 964,
        doi:10.3390/rs12060964, 2020.

Hill, M.: Composition of sea-water comparative and descriptive oceanography, vol. 2, Harvard University Press, USA, 2005.

Hu, C., Lee, Z., and Franz, B.: Chlorophyll-a algorithms for oligotrophic oceans: a novel approach based on three-band reflectance difference,
        Journal of Geophysical Research: Oceans, 117, C01 011, doi:10.1029/2011JC007395, 2012.

535   Huang, P., Lin, I.-I., Chou, C., and Huang, R.-H.: Change in ocean subsurface environment to suppress tropical cyclone intensification under
        global warming, Nature Communications, 6, 7188, doi:10.1038/ncomms8188, 2015.

Hung, C.-C., Gong, G.-C., Lee, M.-A., Liao, C.-H., Chang, Y., Shih, Y.-Y., Chen, K.-S., Chen, M.-H., and Santschi, P. H.: Impacts of
        typhoons on nutrient supply and potential fish production in the Southern East China Sea, in: Typhoon Impact and Crisis Management,
        pp. 267–282, Springer, 2014.

540   Jaimes, B. and Shay, L. K.: Mixed layer cooling in mesoscale oceanic eddies during Hurricanes Katrina and Rita, Monthly Weather Review,
        137, 4188–4207, 2009.

Jaimes, B. and Shay, L. K.: Enhanced wind-driven downwelling flow in warm oceanic eddy features during the intensification of Tropical Cyclone Isaac (2012): Observations and theory, Journal of Physical Oceanography, 45, 1667–1689, 2015.

Jayaram, C., Bhaskar, T. U., Kumar, J. P., and Swain, D.: Cyclone enhanced chlorophyll in the Bay of Bengal as evidenced from satellite and
545   BGC-Argo float observations, Journal of the Indian Society of Remote Sensing, 47, 1875–1882, 2019.

Jullien, S., Menkès, C. E., Marchesiello, P., Jourdain, N. C., Lengaigne, M., Koch-Larrouy, A., Lefèvre, J., Vincent, E., and Faure, V.: Impact of tropical cyclones on the heat budget of the South Pacific Ocean, Journal of Physical Oceanography, 42, 1882–1906, 2012.

Kleckner, R. C. and McCleave, J. D.: The northern limit of spawning by Atlantic eels (*Anguilla* spp.) in the Sargasso Sea in relation to thermal fronts and surface water masses, Journal of Marine Research, 46, 647–667, 1988.

550   Klotzbach, P. J., Schreck III, C. J., Collins, J. M., Bell, M. M., Blake, E. S., and Roache, D.: The extremely active 2017 North Atlantic hurricane season, Monthly Weather Review, 146, 3425–3443, 2018.

Klotzbach, P. J., Bell, M. M., and Jones, J.: Summary of 2019 Atlantic tropical cyclone activity and verification of authors' seasonal and two-week forecasts , Department of Atmospheric Science Colorado State University, https://tropical.colostate.edu/archive-of-past-forecasts, 2019.

555   Knutson, T. R., McBride, J. L., Chan, J., Emanuel, K., Holland, G., Landsea, C., Held, I., Kossin, J. P., Srivastava, A., and Sugi, M.: Tropical cyclones and climate change, Nature Geoscience, 3, 157–163, 2010.

Kossin, J. P.: A global slowdown of tropical-cyclone translation speed, Nature, 558, 104–107, 2018.

Kwon, Y.-O. and Riser, S. C.: North Atlantic Subtropical Mode Water: a history of ocean-atmosphere interaction 1961–2000, Geophysical Research Letters, 31, L19 307, doi:10.1029/2004GL021116, 2004.

560   Laffoley, D. d., Roe, H., Angel, M., Ardron, J., Bates, N., Boyd, L., Brooke, S., Buck, K. N., Carlson, C., Causey, B., et al.: The protection and management of the Sargasso Sea: the golden floating rainforest of the Atlantic Ocean , Sargasso Sea Alliance, USA., 2011.

Lamouroux, J., Perruche, C., Mignot, A., Paul, J., and Szczypta, C.: Quality information document for Global Bio-geochemical Analysis and Forecast product , Issue: 1.0. Copernicus Marine Environment Monitoring Service, http://marine.copernicus.eu/documents/QUID/CMEMS-GLO-QUID-001-028.pdf, 2019.

565   Latasa, M., Gutiérrez-Rodríguez, A., Cabello, A. M. M., and Scharek, R.: Influence of light and nutrients on the vertical distribution of marine phytoplankton groups in the deep chlorophyll maximum, Scientia Marina, 80, 57–62, 2016.

Lawrence, M. B. and Clark, G. B.: Atlantic hurricane season of 1984, Monthly Weather Review, 113, 1228–1237, 1985.

Leipper, D. F. and Volgenau, D.: Hurricane heat potential of the Gulf of Mexico, Journal of Physical Oceanography, 2, 218–224, 1972.

Lellouche, J.-M., Legalloudec, O., Regnier, C., Levier, B., Greiner, E., and Drevillon, M.: Quality information document
570   for Global Sea Physical Analysis and Forecasting product, Issue: 2.1. Copernicus Marine Environment Monitoring Service, http://marine.copernicus.eu/documents/QUID/CMEMS-GLO-QUID-001-024.pdf, 2016.

Lenzen, M., Malik, A., Kenway, S., Daniels, P., Lam, K. L., and Geschke, A.: Economic damage and spillovers from a tropical cyclone, Natural Hazards and Earth System Sciences, 19, 137–151, doi:10.5194/nhess-19-137-2019, 2019.

Liccardo, A., Fierro, A., Iudicone, D., Bouruet-Aubertot, P., and Dubroca, L.: Response of the deep chlorophyll maximum to fluctuations in
575   vertical mixing intensity, Progress in Oceanography, 109, 33–46, 2013.

Lim, Y.-K., Schubert, S. D., Kovach, R., Molod, A. M., and Pawson, S.: The roles of climate change and climate variability in the 2017 Atlantic hurricane season, Scientific Reports, 8, 16 172, doi:10.1038/s41598-018-34343-5, 2018.

Lin, T.-C., Hogan, J. A., and Chang, C.-T.: Tropical cyclone ecology: a scale-link perspective, Trends in Ecology & Evolution, doi:10.1016/j.tree.2020.02.012, 2020.

580   Lin, Y.-C. and Oey, L.-Y.: Rainfall-enhanced blooming in typhoon wakes, Scientific Reports, 6, 31310, doi:10.1038/srep31310, 2016.

Macías, D., Rodríguez Santana, Á., Ramírez-Romero, E., Bruno, M., Pelegrí Llopart, J. L., Sangrà, P., Aguiar González, M. B., and García, C. M.: Turbulence as a driver for vertical plankton distribution in the subsurface upper ocean, Scientia Marina, 77, 541–549, doi:10.3989/scimar.03854.03A, 2013.

Malone, T. C., Pike, S. E., and Conley, D. J.: Transient variations in phytoplankton productivity at the JGOFS Bermuda time series station,
585   Deep Sea Research Part I: Oceanographic Research Papers, 40, 903–924, 1993.

Menkes, C. E., Lengaigne, M., Lévy, M., Éthé, C., Bopp, L., Aumont, O., Vincent, E., Vialard, J., and Jullien, S.: Global impact of tropical cyclones on primary production, Global Biogeochemical Cycles, 30, 767–786, 2016.

Meyers, P. C., Shay, L. K., and Brewster, J. K.: Development and analysis of the systematically merged Atlantic regional temperature and salinity climatology for oceanic heat content estimates, Journal of Atmospheric and Oceanic Technology, 31, 131–149, 2014.

590   Michaels, A. F., Siegel, D. A., Johnson, R. J., Knap, A. H., and Galloway, J. N.: Episodic inputs of atmospheric nitrogen to the Sargasso Sea: contributions to new production and phytoplankton blooms, Global Biogeochemical Cycles, 7, 339–351, 1993.

Mignot, A., Claustre, H., d'Ortenzio, F., Xing, X., Poteau, A., and Ras, J.: From the shape of the vertical profile of in vivo fluorescence to chlorophyll-a concentration, Biogeosciences, 8, 2391–2406, 2011.

Mignot, A., Claustre, H., Uitz, J., Poteau, A., d'Ortenzio, F., and Xing, X.: Understanding the seasonal dynamics of phytoplankton biomass
595   and the deep chlorophyll maximum in oligotrophic environments: A Bio-Argo float investigation, Global Biogeochemical Cycles, 28, 856–876, 2014.

Miller, M. J., Feunteun, E., and Tsukamoto, K.: Did a "perfect storm" of oceanic changes and continental anthropogenic impacts cause northern hemisphere anguillid recruitment reductions?, ICES Journal of Marine Science, 73, 43–56, 2016.

Miller, M. J., Westerberg, H., Sparholt, H., Wysujack, K., Sørensen, S. R., Marohn, L., Jacobsen, M. W., Freese, M., Ayala, D. J.,
600   Pohlmann, J.-D., et al.: Spawning by the European eel across 2000 km of the Sargasso Sea, Biology Letters, 15, 20180835, doi:10.1098/rsbl.2018.0835, 2019a.

Miller, P., Kumar, A., Mote, T., Moraes, F., and Mishra, D.: Persistent hydrological consequences of Hurricane Maria in Puerto Rico, Geophysical Research Letters, 46, 1413–1422, 2019b.

Moeller, H. V., Laufkötter, C., Sweeney, E. M., and Johnson, M. D.: Light-dependent grazing can drive formation and deepening of deep
605   chlorophyll maxima, Nature Communications, 10, 1978, doi:10.1038/s41467-019-09591-2, 2019.

Morel, A.: In-water and remote measurements of ocean color, Boundary-Layer Meteorology, 18, 177–201, 1980.

Morey, S. L., Bourassa, M. A., Dukhovskoy, D. S., and O'Brien, J. J.: Modeling studies of the upper ocean response to a tropical cyclone, Ocean Dynamics, 56, 594–606, 2006.

Morozov, E. G. and Velarde, M. G.: Inertial oscillations as deep ocean response to hurricanes, Journal of Oceanography, 64, 495–509, 2008.

610   Munk, P., Hansen, M. M., Maes, G. E., Nielsen, T. G., Castonguay, M., Riemann, L., Sparholt, H., Als, T. D., Aarestrup, K., Andersen, N. G., et al.: Oceanic fronts in the Sargasso Sea control the early life and drift of Atlantic eels, Proceedings of the Royal Society B: Biological Sciences, 277, 3593–3599, 2010.

Neely, W.: The greatest and deadliest hurricanes of the Caribbean and the Americas: the stories behind the great storms of the North Atlantic, iUniverse, Bloomington, Indiana, USA, 2016.

615   Nigam, T., Prakash, K. R., and Pant, V.: An assessment of the impact of oceanic initial conditions on the interaction of upper ocean with the tropical cyclones in the Arabian Sea, Journal of Operational Oceanography, 13, 121–137, doi:10.1080/1755876X.2019.1658567, 2019.

Ning, J., Xu, Q., Feng, T., Zhang, H., and Wang, T.: Upper ocean response to two sequential tropical cyclones over the northwestern Pacific Ocean, Remote Sensing, 11, 2431, doi:10.3390/rs11202431, 2019.

Oey, L. Y., Ezer, T., Wang, D. P., Fan, S. J., and Yin, X. Q.: Loop Current warming by Hurricane Wilma, Geophysical Research Letters, 33, doi:10.1029/2006GL025873, 2006.

Oey, L. Y., Ezer, T., Wang, D. P., Yin, X. Q., and Fan, S. J.: Hurricane-induced motions and interaction with ocean currents, Continental Shelf Research, 27, 1249–1263, 2007.

Paerl, H. W., Hall, N. S., Hounshell, A. G., Luettich, R. A., Rossignol, K. L., Osburn, C. L., and Bales, J.: Recent increase in catastrophic tropical cyclone flooding in coastal North Carolina, USA: long-term observations suggest a regime shift, Scientific Reports, 9, 10 620, doi:10.1038/s41598-019-46928-9, 2019.

Pasch, R., Kimberlain, T., and Stewart, S.: Tropical cyclone preliminary report Hurricane Floyd, 7–17 September, 1999, National Hurricane Center, https://www.nhc.noaa.gov/data/tcr, 1999.

Pedrosa-Pàmies, R., Conte, M., Weber, J., and Johnson, R.: Carbon cycling in the Sargasso Sea water column: insights from lipid biomarkers in suspended particles, Progress in Oceanography, 168, 248–278, 2018.

Prakash, K. R., Nigam, T., and Pant, V.: Estimation of oceanic subsurface mixing under a severe cyclonic storm using a coupled atmosphere-ocean-wave model., Ocean Science, 14, 259–272, 2018.

Price, J. F.: Upper ocean response to a hurricane, Journal of Physical Oceanography, 11, 153–175, 1981.

Price, J. F.: Metrics of hurricane-ocean interaction: vertically-integrated or vertically-averaged ocean temperature?, Ocean Science, 5, 351–368, 2009.

Reverdin, G., Molinari, R., and Du Penhoat, Y.: Objective analysis of thermocline depth distributions obtained in the tropical Atlantic Ocean during FGGE, 1979, Deep Sea Research Part A. Oceanographic Research Papers, 33, 43–53, 1986.

Riemann, L., Alfredsson, H., Hansen, M. M., Als, T. D., Nielsen, T. G., Munk, P., Aarestrup, K., Maes, G. E., Sparholt, H., Petersen, M. I., et al.: Qualitative assessment of the diet of European eel larvae in the Sargasso Sea resolved by DNA barcoding, Biology Letters, 6, 819–822, 2010.

Santer, B. D., Wigley, T., Gleckler, P., Bonfils, C., Wehner, M., AchutaRao, K., Barnett, T., Boyle, J., Brüggemann, W., Fiorino, M., et al.: Forced and unforced ocean temperature changes in Atlantic and Pacific tropical cyclogenesis regions, Proceedings of the National Academy of Sciences, 103, 13 905–13 910, 2006.

Schmidt, J.: The breeding places of the eel, Philosophical Transactions of the Royal Society of London. Series B, Containing Papers of a Biological Character, 211, 179–208, 1923.

Schroeder, E., Stommel, H., Menzel, D., and Sutcliffe Jr, W.: Climatic stability of eighteen degree water at Bermuda, Journal of Geophysical Research, 64, 363–366, 1959.

Seager, R., Cane, M., Henderson, N., Lee, D.-E., Abernathey, R., and Zhang, H.: Strengthening tropical Pacific zonal sea surface temperature gradient consistent with rising greenhouse gases, Nature Climate Change, 9, 517–522, 2019.

Shay, L. K., Brewster, J. K., Maturi, E., Donahue, D., Meyers, P., and McCaskill, C.: Algorithm theoretical basis document for satellite derived oceanic heat content product version 3.2. ATBD: satellite-derived oceanic heat content product, NOAA /RSMAS https://www.ospo.noaa.gov/Products/ocean/assets/ATBD_OHC_NESDIS _V3.2.pdf, 2019.

Shi, W. and Wang, M.: Observations of a Hurricane Katrina-induced phytoplankton bloom in the Gulf of Mexico, Geophysical Research Letters, 34, L11 607, doi:10.1029/2007GL029724, 2007.

Shropshire, T., Li, Y., and He, R.: Storm impact on sea surface temperature and chlorophyll a in the Gulf of Mexico and Sargasso Sea based
655   on daily cloud-free satellite data reconstructions, Geophysical Research Letters, 43, 12 199–12 207, 2016.

Song, J., Klotzbach, P. J., Tang, J., and Wang, Y.: The increasing variability of tropical cyclone lifetime maximum intensity, Scientific
Reports, 8, 16 641, doi:10.1038/s41598-018-35131-x, 2018.

Steinberg, D. K., Carlson, C. A., Bates, N. R., Johnson, R. J., Michaels, A. F., and Knap, A. H.: Overview of the US JGOFS Bermuda
Atlantic Time-series Study (BATS): a decade-scale look at ocean biology and biogeochemistry, Deep Sea Research Part II: Topical
660   Studies in Oceanography, 48, 1405–1447, 2001.

Stevens, S. W., Johnson, R. J., Maze, G., and Bates, N. R.: A recent decline in North Atlantic subtropical mode water formation, Nature
Climate Change, 10, 335–341, 2020.

Stewart, S. R.: Tropical cyclone report Hurricane Humberto, 13–19 September 2019, National Hurricane Center,
https://www.nhc.noaa.gov/data/tcr, 2020.

665   Sun, Y., Zhong, Z., Li, T., Yi, L., Hu, Y., Wan, H., Chen, H., Liao, Q., Ma, C., and Li, Q.: Impact of ocean warming on tropical cyclone size
and its destructiveness, Scientific Reports, 7, 8154, doi:10.1038/s41598-017-08533-6, 2017.

Trenberth, K. E., Cheng, L., Jacobs, P., Zhang, Y., and Fasullo, J.: Hurricane Harvey links to ocean heat content and climate change adaptation,
Earth's Future, 6, 730–744., 2018.

Trepanier, J. C.: North Atlantic hurricane winds in warmer than normal seas, Atmosphere, 11, 293, doi:10.3390/atmos11030293, 2020.

670   van Ginneken, V. J. and Maes, G. E.: The European eel (*Anguilla anguilla*, Linnaeus), its lifecycle, evolution and reproduction: a literature
review, Reviews in Fish Biology and Fisheries, 15, 367–398, 2005.

Vincent, E. M., Lengaigne, M., Madec, G., Vialard, J., Samson, G., Jourdain, N. C., Menkes, C. E., and Jullien, S.: Processes set-
ting the characteristics of sea surface cooling induced by tropical cyclones, Journal of Geophysical Research: Oceans, 117, C02 020,
doi:10.1029/2011JC007396, 2012a.

675   Vincent, E. M., Lengaigne, M., Vialard, J., Madec, G., Jourdain, N. C., and Masson, S.: Assessing the oceanic control on the amplitude of
sea surface cooling induced by tropical cyclones, Journal of Geophysical Research: Oceans, 117, C05 023, doi:10.1029/2011JC007705,
2012b.

Walker, N. D., Leben, R. R., and Balasubramanian, S.: Hurricane-forced upwelling and chlorophyll a enhancement within cold-core cyclones
in the Gulf of Mexico, Geophysical Research Letters, 32, doi:10.1029/2005GL023716, 2005.

680   Walsh, K. J., McBride, J. L., Klotzbach, P. J., Balachandran, S., Camargo, S. J., Holland, G., Knutson, T. R., Kossin, J. P., Lee, T.-c., Sobel,
A., et al.: Tropical cyclones and climate change, Wiley Interdisciplinary Reviews: Climate Change, 7, 65–89, 2016.

Wang, T., Zhang, S., Chen, F., MA, Y., Jiang, C., and Yu, J.: Influence of sequential tropical cyclones on phytoplankton blooms in the
northwestern South China Sea, Chinese Journal of Oceanology and Limnology, doi:10.1007/s00343-020-9266-7, 2020.

Wei, J., Liu, X., and Jiang, G.: Parameterizing sea surface temperature cooling induced by tropical cyclones using a multivariate linear
685   regression model, Acta Oceanologica Sinica, 37, 1–10, 2018.

Welker, C. S. and Faust, E.: Tropical cyclone-related socio-economic losses in the western North Pacific region, Natural Hazards and Earth
System Sciences, 13, 115–124, 2013.

Wu, R. and Li, C.: Upper ocean response to the passage of two sequential typhoons, Deep Sea Research Part I: Oceanographic Research
Papers, 132, 68–79, 2018.

690   Wu, Y., Platt, T., Tang, C. C., and Sathyendranath, S.: Short-term changes in chlorophyll distribution in response to a moving storm: a
modelling study, Marine Ecology Progress Series, 335, 57–68, 2007.

Ye, H., Sui, Y., Tang, D., and Afanasyev, Y.: A subsurface chlorophyll a bloom induced by typhoon in the South China Sea, Journal of Marine Systems, 128, 138–145, 2013.

Zanna, L., Khatiwala, S., Gregory, J. M., Ison, J., and Heimbach, P.: Global reconstruction of historical ocean heat storage and transport, Proceedings of the National Academy of Sciences, 116, 1126–1131, 2019.

Zhang, H., Chen, D., Zhou, L., Liu, X., Ding, T., and Zhou, B.: Upper ocean response to typhoon Kalmaegi (2014), Journal of Geophysical Research: Oceans, 121, 6520–6535, 2016.

Zhang, L., Karnauskas, K. B., Donnelly, J. P., and Emanuel, K.: Response of the North Pacific tropical cyclone climatology to global warming: application of dynamical downscaling to CMIP5 models, Journal of Climate, 30, 1233–1243, 2017.

Zhao, H., Shao, J., Han, G., Yang, D., and Lv, J.: Influence of typhoon matsa on phytoplankton chlorophyll-a off East China, PloS one, 10, e0137 863, doi:10.1371/journal.pone.0137863, 2015.